AN EDUCATIONAL ANIMATION OF THE PROPAGATION OF EARTHQUAKE–GENERATED SEISMIC SHEAR WAVES ACROSS THE MANTLE

Michael E. Wysession
Department of Earth and Planetary Sciences, Washington University, St. Louis, MO 63130, michael@wucore.wustl.edu

Saadia Baker
Department of Earth and Planetary Sciences, Washington University, St. Louis, MO 63130, saadia@ocean.wustl.edu

ABSTRACT

Computer-generated animations form a powerful tool for geophysical education. The realistic animations, computed from more than 100,000 normal mode synthetic seismograms, show the manner in which seismic shear waves propagate across the mantle from hypothetical earthquakes. The visualizations provide an understanding of seismic wave propagation that cannot be gained from more traditional ray-tracing techniques.

Keywords: Education - computer assisted; Geophysics - Seismology

INTRODUCTION

We know more about the large-scale distribution of galaxies within the universe and small-scale distribution of organelles within a human cell than we do about what is 10 meters beneath us. The reason is simple - light doesn't pass through rock. The field of seismology has therefore played the dominant role in imaging the structure of the Earth from scales of shallow seismic reflection profiling to whole-Earth seismic tomography. Unlike the case of light, which generally deviates only slightly from a straight path due to refraction and diffraction (because of the very small wavelengths involved), the path of seismic waves between sources and receivers within the Earth are usually quite complicated. It is therefore important for Earth scientists to have an understanding of how seismic waves propagate through the Earth, and it is in this context that the seismic wave animations discussed here have been generated.

The field of seismology is surprisingly lacking in high-quality visualization examples of seismic wave propagation due to the extreme analytical and computational challenges involved. Simple approximations using ray-tracing are abundant, but as will be shown, these do not convey the true manner by which seismic waves from earthquakes and other sources travel through the Earth. In the current demonstration we use a normal mode summation algorithm. The result is a complete and fairly accurate representation of the seismic shear wave field within Earth's mantle that would result from earthquakes occurring at different depths. This kind of visualization can provide Earth scientists with a sense of the true style of mantle wave propagation that cannot be gained through other methods such as ray-tracing.

The computer-generated animations, which appear as educational products in both web-based "Shockwave" and VHS formats (see information at end of paper), are run in several different manners to show various aspects of mantle wave propagation. These include the different effects of homogeneous and realistic radial velocity models, shallow and deep earthquakes, and propagation directions relative to the earthquake's focal mechanism. Note that these animations only show the horizontal shear (SH) wave field, and not the coupled compressional/vertical shear (P/SV) wave field, which is much more computationally challenging. It is our hope that these efforts will give future geophysicists a better understanding of the process by which seismic waves sample the Earth, and will encourage other efforts (such as Cummins (1996)) at visually representing the complex propagation of earthquake-generated seismic waves within the Earth.

VISUALIZING WAVES

Visualizing the propagation of waves has long been a challenge to many areas of science. Attempts are often done using the approximation of ray-tracing, whereby the wave is treated as a finite number of discrete particles that follow trajectories obeying Snell's Law. While this gives a general idea of the wave directions, it generally bears little resemblance to the actual wave field being represented (Figure 1). The reason, of course, is that waves are not agglomerations of particles, and while they do not disobey Snell's Law, they display all sorts of other additional interesting behaviors such as diffraction and interference.

Another approach to the use of ray-tracing is to not show the hypothetical ray paths, but instead show the wave front formed by connecting the leading ray tips at successive intervals. This technique has been used in some very nice educational animations, such as the program "Seismic Waves" (A. Jones, personal communication). However, while this technique provides a good sense of mantle wave refraction, it is still only as complete as the seismic phases chosen to be traced, and does not show the wave amplitudes.

An alternative formulation would be to use the description given by Huygens himself and treat the wave front as a set of infinite points, each of which acts as a point source generator of overlapping spherical waves. An example is shown in Figure 2. To maintain a realistic

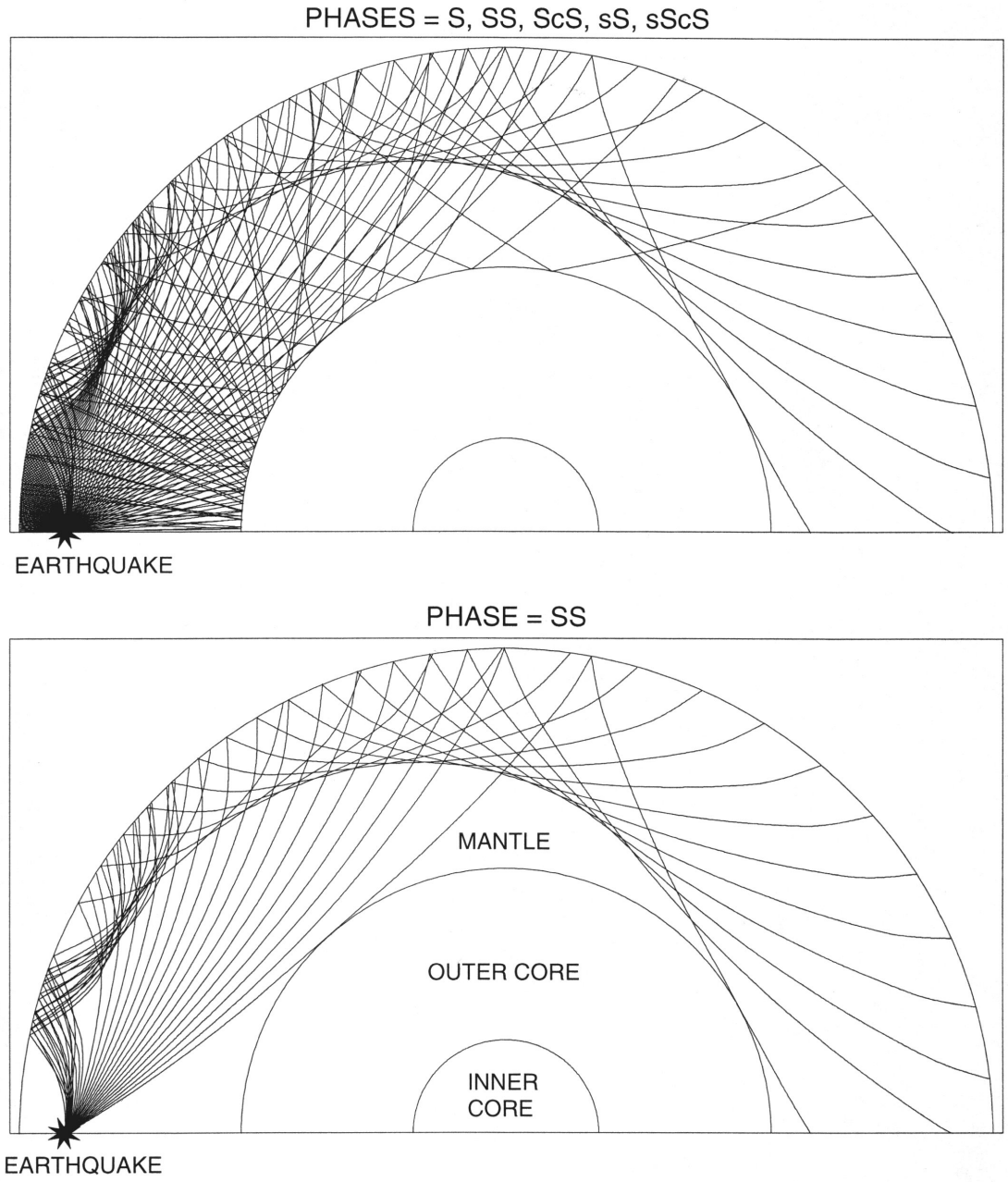

Figure 1. Two representations of seismic shear waves in the mantle using ray-tracing. The top panel shows the rays generated for a suite of seismic phases at 2° increments in take-off angles from a 600-km deep earthquake, and it appears as a jumbled mess. In addition to not being a complete representation of the seismic shear wave field, there is no sense of time history to the waves, and only qualitative information about amplitudes. The bottom panel shows a similar image, but for only one phase, the surface-reflected SS wave. Here, there is a better sense of the wave direction and of the change in refractive index of the mantle as a function of depth. However, note that the striking boundary made by the superposition of lines, called a caustic, is in this case an artifact of the lack of time history of the waves. Ray-tracing has always been the predominant means of visualizing seismic waves due to its computational simplicity.

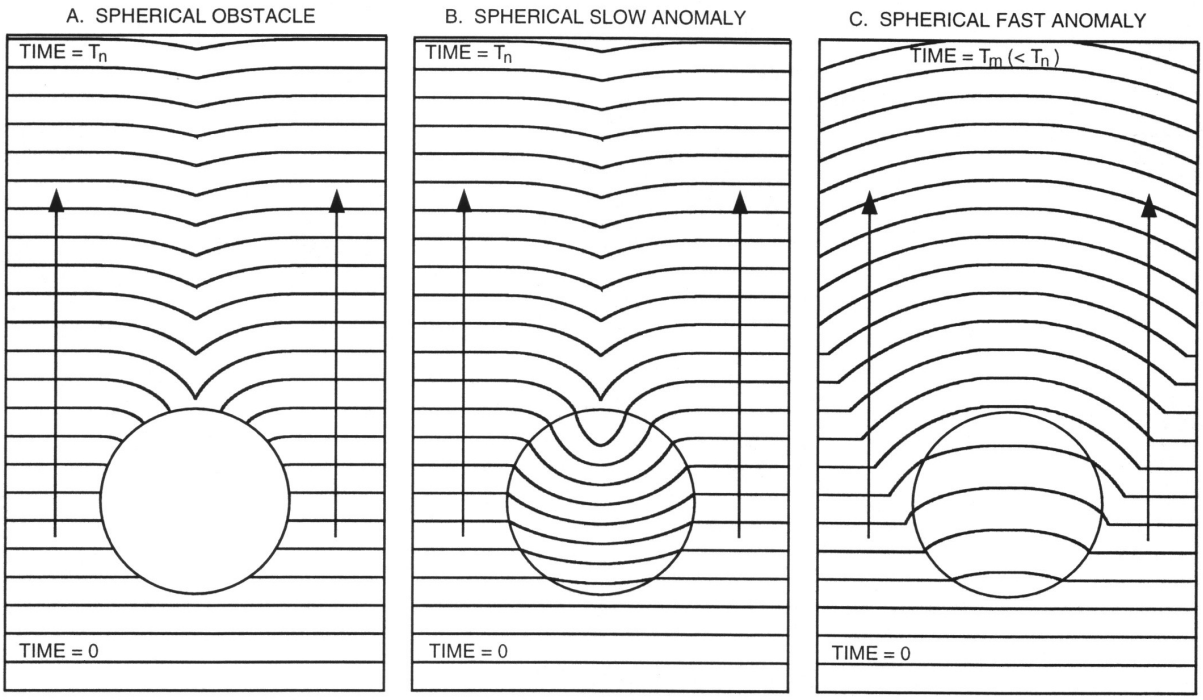

Figure 2. Demonstration of representing waves as the leading front of the superposition of Huygens point sources, here shown for waves interacting with a spherical anomaly of differing relative velocities. This formulation is able to show how a straight wave front coming in contact with a circular or spherical obstacle diffracts around it, a process not described by geometric ray theory and therefore not present in ray-tracing. Because of the difficulty in treating the waves as an ever increasing set of point sources, only the leading wave front is shown, and there is no quantitative information about wave amplitudes.

wave representation, however, it is easy to see that the computational requirements of keeping track of the rapidly increasing number of points is staggering. If computational brute force is to be used, the best technique is to break the region of interest into a three-dimensional grid of points. These points are "connected" to each other by physical laws of material properties such as rigidity and incompressibility that can determine how the region would respond elastically to a given disturbance. The ability of this method, called finite difference modeling, to represent wave propagation is therefore dependent upon the number of grid nodes used, and therefore the computational power available. This technique is most commonly used to look at regional crustal wave propagation (e.g., Frankel and Vidale, 1992; Graves and Clayton, 1992; Frankel, 1993; Zhang et al., 1998; Korneev et al., 2000), where it can include effects of boundary topography and three-dimensional heterogeneity. Finite difference techniques are just now beginning to be used on a whole-Earth scale (Igel and Weber, 1996; Thomas et al., 2000), and with expected advances in computational power, will most likely be the favorite technique for future applications. There are other mathematical techniques that can be used to show wave propagation through a region, such as use of the Born approximation (e.g., Dalkolmo and Friederich, 2000) and generalized screen propagator methods (e.g., Wu et al., 2000), but these do not provide the full wave fields.

A different approach is to treat the full wave history of the whole Earth as a unique sum of normal modes of oscillation. It is a physical property that any wave can be described either as a time series of displacements ("time domain") or as a sum of the orthogonal modes of oscillation of the system ("frequency domain"). For example, you could describe the sound of a hammer striking a piano string as a time signal, like an audio tape recording. Alternately, you could describe the "sound" of the string as a summation of the fundamental note and all of the associated harmonic overtones, which is what an electronic synthesizer does. The two formulations are, of course, equivalent because nature, whose displacement field is real, knows nothing about time and frequency domains, which are purely human constructs. The advantage of the frequency-domain formulation is that the complete wave field is generated. The disadvantage is that the wave field is only as precise as the frequency to which modes are computed, and the computation of modes for all but the simplest of geometries is non-trivial.

A simple example of mode summation is shown in Figure 3 for one-dimensional wave propagation on a string of two different densities. The complete history of

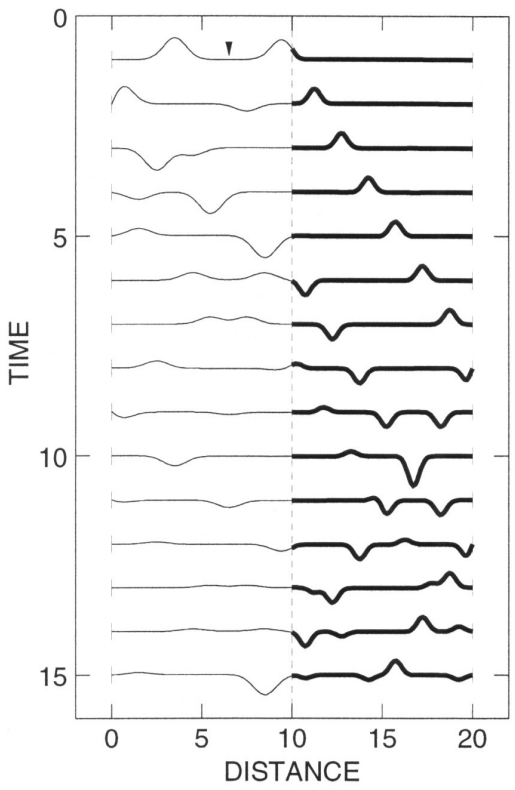

Figure 3. Example of wave propagation generated by the summation of normal modes, here for the one- dimensional case of wave propagation on a string composed of two segments of different properties: the left with a relative density of 1 and velocity of 3, and the right with a density of 4 and velocity of 1.5. The different traces are snapshots of the string at successive times one time unit apart. The vertical dashed line indicates the position of the junction, and both ends of the string are fixed. The complete time history of the string displacements is produced by the normal mode summation. (Courtesy of S. Stein)

the successive reflections and transmissions of waves across the two string segments is obtained through a summation of the harmonic overtones of the string. Because amplitudes are now accurately represented, a visualization of this system (Stein and DeLaughter, 1997) has a realistic appearance.

MANTLE SHEAR WAVE PROPAGATION

In our visualization of mantle shear waves, all modes (28,588) of torsional Earth oscillations with periods longer than 12 s are computed and then summed at the appropriate proportions for particular earthquake depths and focal mechanisms. In all cases a simple rupture along a fault, modeled by a double-couple of forces, is used to represent the earthquake. Details of the analytical formulation are given in Wysession and Shore (1995). A grid of 111,687 nodes, separated by 20 km, is constructed for a hemispherical slice through the mantle, and a synthetic seismogram is computed at each node. The computation time is much less than for the finite difference model. Because shear waves do not pass through liquids, the SH waves do not pass into the core. The animation is created by taking successive time slices of the displacement field formed by the large grid of synthetic seismograms.

We repeat the process for different conditions in order to demonstrate different aspects of mantle wave propagation. While most of the animations are done using a realistic radial model of seismic velocities (Dziewonski and Anderson, 1981), we start with the hypothetical case of a homogeneous mantle of constant seismic velocity. The wave field, while broken up by reflections off of the surface, core, and mid-mantle discontinuities, travels across the mantle in a fairly concentrated manner. In contrast, the general increase in seismic velocities with depth (due to compression) in the realistic Earth model makes the different segments of the wave field for these examples greatly diverge from each other. The initially spherical wave front leaving the earthquake source soon becomes a complicated suite of displacements. In seismological practice we give each of these different branches of the seismic shear wave field a different name (such as S, SS, sS, ScS, SSS, sSS, etc.), and it is easy to forget that they originate from a single spherical shear wave front.

Some examples are shown for the case of a strike-slip earthquake on a dipping fault at a depth of 600 km (Figure 4). The calculations show accurate relative amplitudes, which have been raised to a power of 0.8 to enhance smaller signals. Dark shades represent displacements out of the paper, and light shades are displacements into the paper. In the first panel, Figure 4a, which is 60 s after the earthquake occurs, the wave front still maintains much of its initially spherical shape. The vertically-rising wave front is headed toward the surface, but will not reach it for another 67 s. The bottom part of the wave front is headed toward the core, where it will be fully reflected. This ScS wave will reach the surface directly above the earthquake 808 s after the earthquake occurred. The dark shaded region that seems to precede the initial wave is the artifact created by the truncation of our normal modes at periods of less than 12 s. If we could go to smaller periods, this artifact would disappear.

In Figure 4b, 300 s after the earthquake, the wave front still maintains its integrity, though the upper part is now reflecting off of the surface, and the lower part is about to reach the core. Slow upper mantle velocities can be seen in the bends that occur in both the reflected and unreflected waves. The S wave front is currently in contact with the surface 12.5° away from the source, and at closer distances has already left the surface. When these waves reach the surface again, they will be called the sS and sScS phases.

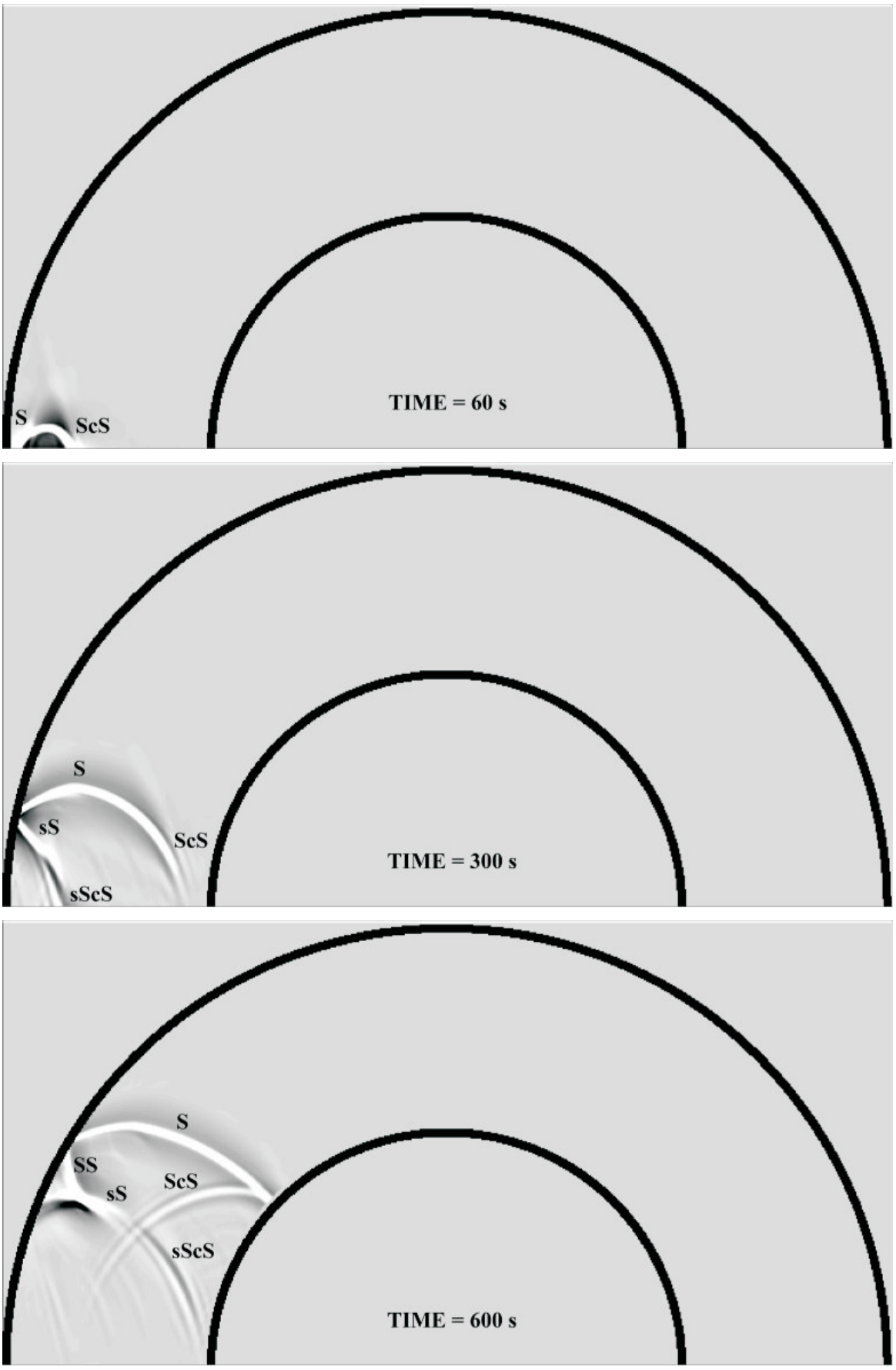
S
ScS
TIME = 60 s
S
sS
ScS
sScS
TIME = 300 s
S
SS
sS
ScS
sScS
TIME = 600 s

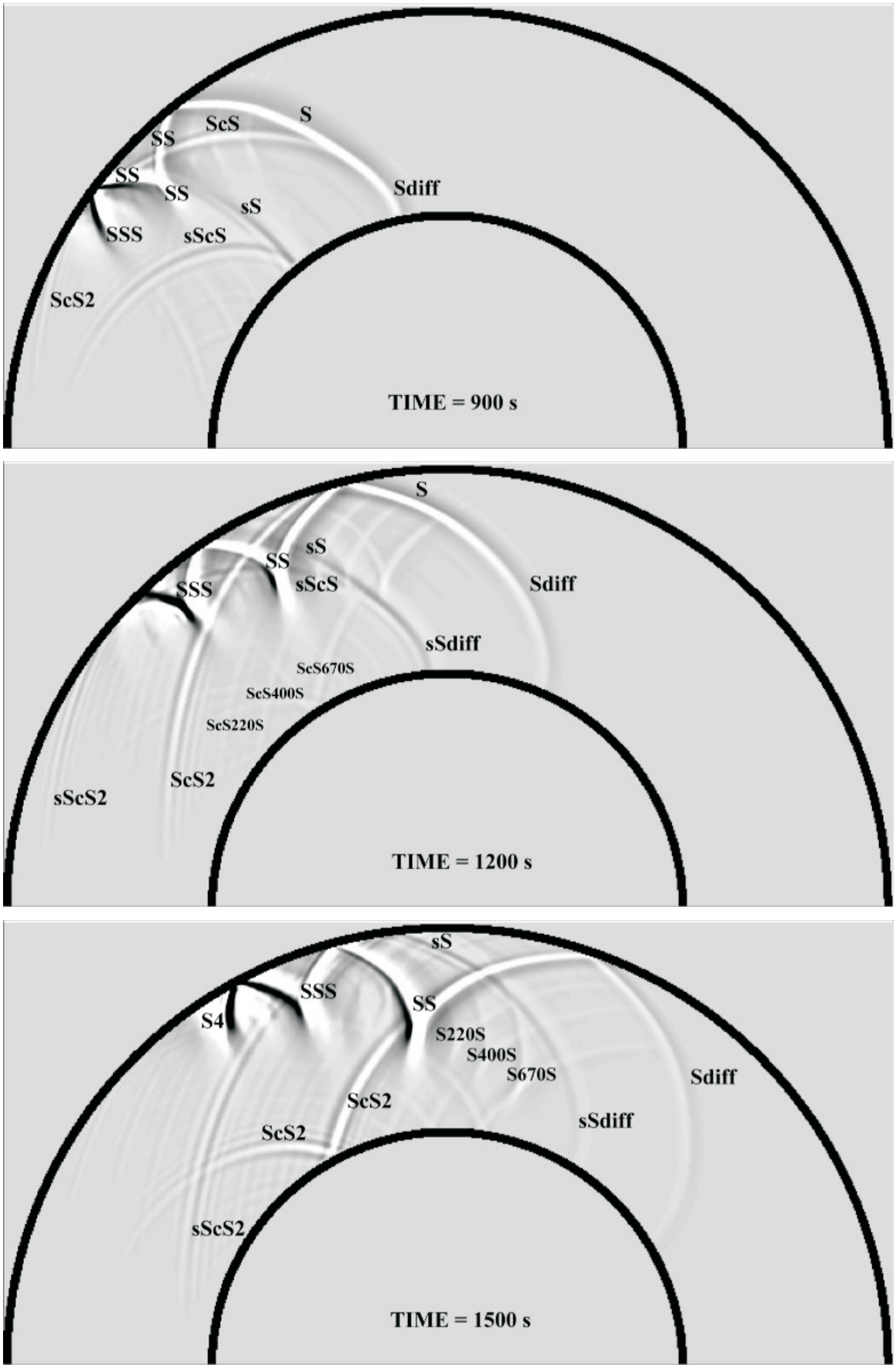
S
ScS
SS
SS
SS
sS
Sdiff
SSS
sScS
ScS2
TIME = 900 s
S
sS
SS
SSS
sScS
Sdiff
sSdiff
ScS670S
ScS400S
ScS220S
ScS2
sScS2
TIME = 1200 s
sS
SSS
SS
S4
S220S
S400S
S670S
Sdiff
ScS2
sSdiff
ScS2
sScS2
TIME = 1500 s

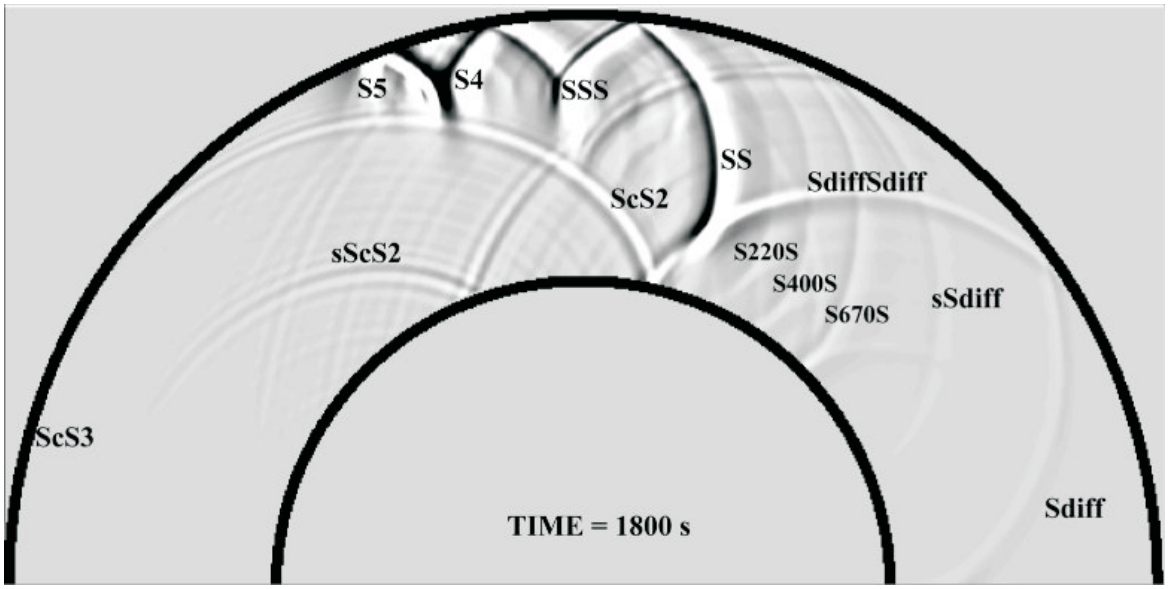

Figure 4. Example of a realistic propagation of seismic shear waves across the mantle from a 600-km deep earthquake, made using a summation of Earth's torsional modes of oscillation. Dark shades represent displacements out of the paper, and light shades are displacements into the paper. Successive panels are series of time slices through a spherically symmetric mantle after the occurrence of a 600-km deep earthquake, showing the propagation of the SH shear waves. The animations show this in a continuous process. The initial wave front moves away from the source, which occurs at the lower left side of the figures. The wave front begins to develop complexity due to interactions with the surface, the core-mantle boundary, and internal discontinuities and velocity gradients. In the video animation, these slices appear continuously in color, and are accompanied by cogenerated seismograms and a descriptive narration.

In Figure 4c, now 600 s after the earthquake, added complexity is evident. The core-reflected wave takes the form of ScS and its multiples (ScS2, ScS3, etc.), but the surface-reflected wave is separating into two parts. One part will head into the lower mantle and eventually reach the surface as the minimum-time sScS and sS phases. The other will turn higher up in the mantle and arrive at the surface as the maximum-time SS phase. Behind the sS, ScS, and sScS wave fronts can be seen upper mantle echoes caused by internal reflections from the 220, 400, and 670 km discontinuities within the Earth model of Dziewonski and Anderson (1981). Use of other Earth models that place these discontinuities at slightly different depths would have an imperceptibly small effect upon the visualization. The only phase yet recorded at the surface is S, now arriving 31.3° away from the source. The sS wave will begin to arrive in another 63 s, at an angular distance of 24.2°.

By 900 s after the origin time, Figure 4d, four segments of the broken wave front have reached the surface: S at 52.4°, sS at 38.9°, SS at 37.9°, and ScS at 32.6°. While the sS and SS waves have begun to separate, the ScS and S waves have begun to come back together. The latter occurs where the wave enters the core shadow, and the S/ScS wave front continues on as a core-diffracted S_{diff} wave. The base of the S_{diff} wave is already 80.7° around the core by this time. Behind the S and ScS waves in the lower mantle are the sS and sScS waves, which follow similar paths except for their surface reflections. The distance between S and sS (and also ScS and sScS) is a function of the depth of the earthquake, which is 600 km in this case. Note that there are three wave segments that are all labeled SS. Together, they form a characteristic "Y" shape that results from having the waves turn in the mid-mantle. The junction represents the superposition of the part of the wave front that is heading down toward the bottoming point and the part of the wave front that has already turned and is heading back up again. Behind SS the phase SSS is beginning to form. This wave bounces twice on the underside of the surface.

In Figure 4e, 1200 s after the earthquake, most of the initial S wave front is actually S_{diff}, because the bottom of the S wave has begun to graze the core. Even the surface-reflected sS wave is now diffracting around the core as sS_{diff}. The phase SSS is now fully developed, and is reaching the surface behind SS. Notice, however, that the polarity of SSS is different from SS. With each successive bounce that that the waves take on the underside of the surface, the phase of the wave is shifted by $\pi/2$, a phenomenon identified for surface-reflected seismic waves. As a result, while the initial S wave is into the page (light-colored), the SSS wave is primarily out of the page (dark colored) because it has been phase-shifted by $2 \times \pi/2$ (once for each of the two surface bounces), and is totally out of phase from the initial wave. There are a lot

of smaller-amplitude phases evident, and these are the reflections off of the upper mantle discontinuities. These smaller phases usually occur in threes from the discontinuities at depths of 220, 400 and 670 km. One set of these, labeled in 4e as ScS220S, ScS400S, and ScS670S, are the underside reflections that precede ScS2.

In Figure 4f, 1500 s after the earthquake, the initial wave is now fully core-diffracted, and reaches the surface at an angular distance of 111.5°. Because waves travel so much faster at the base of the mantle than in the upper mantle, the S_{diff} wave at the core-mantle boundary has already reached an angular distance of 152.5°. Another set of mid-mantle reflections, clearly observed here and in the previous panel (4e), are the precursors to SS called S220S, S400S, and S670S. These can be seen peeling off of the upgoing S/S_{diff} wave front as it interacts with the discontinuities. Because these are related to SS, they also have the Y-shaped structure characteristic of maximum-time underside-reflected phases. In Figure 4f, the upgoing parts of the Y structures were reflected off of the upgoing S phase, but the downgoing parts (right side of the Y) are peeling off of S_{diff}, and are more properly called $S_{diff}200S_{diff}$, $S_{diff}400S_{diff}$, and $S_{diff}670S_{diff}$. The waves with the largest amplitudes are now SS and SSS, which are arriving at the surface at angular distances of 76.4° and 63.3°.

In Figure 4g, 1800 s after the earthquake, S4 has begun to be observed at the surface (70.8°), following SS (97.3°) and SSS (82.6°). The next surface reflection, S5, is now developing. Note the reversal of polarity between SSS and S, which are a full out of phase. The ScS2 multiple reflection is arriving at the surface 36.3° from the earthquake, and at closer distances it is already heading back down to the core as what will later be recorded at the surface as ScS3. The downgoing part of SS is from S_{diff} reflecting at the surface, so it will arrive at the surface at angular distances greater than 200° as phase $S_{diff}S_{diff}$. Thirty minutes have now passed since the earthquake occurred, and seismic shear energy has now spread throughout the mantle. Multiple ScS waves are still reverberating between the surface and core beneath the epicenter, and the leading S_{diff} wave has now wrapped around the antipode and is heading back toward the epicenter. The initially spherical shear wave front has now broken into a great number of separate surfaces.

A significant feature of this exercise is the lack of an obvious core shadow zone. Since geometric ray-tracing cannot describe diffraction (unless it is artificially included), it is easy to think of waves stopping at the edge of an obstacle and to forget that waves diffract around it, as was shown in Figure 2. It is difficult to notice the effect of the core-diffraction upon the S_{diff} waves reaching the surface. The ray parameter of all core-diffracted S_{diff} waves is roughly the same (except for lateral heterogeneities), because they all bottom at the same depth, which is the core-mantle boundary. This means that the S_{diff} wave front always reaches the surface at the same incident angle. There is also a preferential decrease in higher-frequency amplitudes during diffraction, making the S_{diff} wave front less sharply defined. These effects are secondary, however, and the fact remains that while the concept of a shadow zone has many instructional uses, it has long been an artifact of viewing seismic wave propagation with ray tracing instead of wave tracing.

This example does not fully convey the process of wave propagation, but gives some idea of it. In the web-based format, color graphics are used, and sample seismograms that would be simultaneously recorded at angular distances of 30°, 60°, and 90 are shown as well. In addition, the VHS format includes a narration track that describes the animations step-by-step. The example in Figure 4 was for an earthquake at a depth of 600 km. We also include animations at depths of 300 and 20 km, and the latter case is strongly dominated by the surface-trapped Love waves. Another example shows the wave field at an azimuth 180° away in order to show the effect of the azimuthal orientation from the fault in terms of the amplitudes and polarities of the different wave branches, which are different than in the previous examples. This dependence upon azimuth is also shown by an animation where a hypothetical seismometer at an angular distance of 90° from the earthquake is rotated 360° in azimuth around the earthquake source, with the result that the different seismic phases change amplitudes and polarities at different times. Lastly, the presentation shows the contrasting appearances of ray-tracing examples of many of the SH phases shown in the wave propagation animations.

SUMMARY

We present in web and VHS formats examples of the propagation of seismic shear waves from hypothetical earthquakes. The technique of normal mode summation creates a realistic visualization of the manner by which the initially simple wave field from a simple double-couple earthquake rupture becomes the broken and varied shear wave field that is described through the use of many phase labels such as S, SS, ScS, sS, etc. This kind of visualization does a much better job of giving a student a sense of how seismic waves, which are our primary tools for imaging the structure of the interior of the Earth, actually interact with Earth's compositional and mineralogical phase boundaries. Examples of the more traditional ray-tracing technique, also included for contrast, show complementary aspects of the wave propagation. The strength of the ray-tracing is to show the effect of refraction along a wave path. The animations of true wave propagation, however, show many phenomena not evident with ray-tracing, such as diffraction of waves around the core and relative amplitudes of all

phases involved. One of the most striking observations, in direct contrast to pedagogical presentations in most textbooks, is the lack of a physical core "shadow zone" due to the continuous diffraction of waves around the core.

ACKNOWLEDGMENTS

Helpful support was provided by Ghassan Aleqabi and Patrick Shore, and the text owes much to discussions with Seth Stein. The project was funded by a David and Lucile Packard Foundation Fellowship for Science and Engineering, an NSF Presidential Faculty Fellowship (NSF-EAR-9629018), and an NSF Division of Undergraduate Education grant (NSF-DUE-9455417).

REFERENCES

Cummins, P., 1996, Observation and modeling of near field earthquake effects at teleseismic distances: Eos, Transactions, American Geophysical Union, v. 77, p. F54.

Dalkolmo, J., and W. Friederich, 2000, Born scatterers of long-period body waves: Geophysical Journal International, v. 142, p. 876-888.

Dziewonski, A. M., and D. L. Anderson, 1981, Preliminary reference Earth model: Physics of the Earth and Planeary Interiors, v. 25, p. 297-356.

Frankel, A., 1993, Three-dimensional simulations of ground motions in the San Bernardino Valley, California, for hypothetical earthquakes on the San Andreas fault: Bulletin of the Seismological Society of America, v. 83, p. 1020-1041.

Frankel, A., and J. Vidale, 1992, A three-dimensional simulation of seismic waves in the Santa Clara Valley, California, from a Loma Prieta aftershock: Bulletin of the Seismological Society of America, v. 82, p. 2045-2074.

Graves, R. W., and R. W. Clayton, 1992, Modeling path effects in three-dimensional basin structures: Bulletin of the Seismological Society of America, v. 82, p. 81-103.

Korneev, V. A., T. V. McEvilly, and E. D. Karageorgi, 2000, Seismological studies at Parkfield VIII: Modeling the observed travel-time changes: Bulletin of the Seismological Society of America, v. 90, p. 702-708.

Igel, H. and M. Weber, 1996, P-SV wave propagation in the Earth's mantle using finite differences; application to heterogeneous lowermost mantle structure: Geophysical Research Letters, v. 23, p. 415-418.

Stein, S. and J. DeLaughter, 1997, Upgrading a beginning geophysics course: taking a "small-is-beautiful" approach: Eos, v. 78, p. 521-532.

Thomas, C., H. Igel, M. Weber, and F. Scherbaum, 2000, Acoustic simulation of P-wave propagation in a heterogeneous spherical earth: numerical method and application to precursor waves to PKPdf: Geophysical Journal International, v. 141, p. 307-320.

Wu, R.-S., S. Jin, and X.-B. Xie, 2000, Seismic wave propagation and scattering in heterogeneous crustal waveguides using screen propagators: I SH waves: Bulletin of the Seismological Society of America, v. 90, p. 401-413.

Wysession. M. E., and P. Shore, 1994, Visualization of whole mantle propagation of seismic shear energy using normal mode summation: Pure and Applied Geophysics, v. 142, p. 295-310.

Zhang, B., A. S. Papageorgiou, and J. L. Tassoulas, 1998, A hybrid numerical technique, combining the finite-element and boundary-element methods: Bulletin of the Seismological Society of America, v. 88, p. 1036-1050.

About the Author

Michael Wysession is an Associate Professor in the Department of Earth and Planetary Sciences at Washington University. His main area of research involves using seismic waves to investigate the structure and composition of the core-mantle boundary, and he is currently installing an IRIS PASSCAL array of seismometers from Florida to Edmonton, Canada, in order to examine mantle structure from the surface to the core. He is a co-author on a textbook entitled "Introduction to Seismology, Earthquakes, and Earth Structure," currently in press with Blackwell Scientific. Educators may obtain a free VHS video copy of the movie by sending an addressed label to the first author. Animations are available on-line at http://epsc.wustl.edu/seismology/michael/movie.html [The other web sites referred to in this paper are the "Seismic Waves" program of A. Jones, at http://www.geol.binghamton.edu/faculty/jones, and the string propagation visualization of (Stein and DeLaughter, 1997), at http://www.earth.nwu.edu/people/seth/demos/STRING/string.html.]